

Electron-hole asymmetry in the superconductivity of doped BaFe_2As_2 seen via the rigid chemical-potential shift in photoemission

M. Neupane,¹ P. Richard,^{2,3} Y.-M. Xu,¹ K. Nakayama,⁴ T. Sato,⁴ T. Takahashi,^{2,4} A. V. Federov,⁵ G. Xu,³ X. Dai,³ Z. Fang,³ Z. Wang,¹ G.-F. Chen,¹ N.-L. Wang,³ H.-H. Wen,³ and H. Ding³

¹*Department of Physics, Boston College, Chestnut Hill, Massachusetts 02467, USA*

²*WPI Research Center, Advanced Institute for Materials Research, Tohoku University, Sendai 980-8577, Japan*

³*Beijing National Laboratory for Condensed Matter Physics, and Institute of Physics, Chinese Academy of Sciences, Beijing 100190, China*

⁴*Department of Physics, Tohoku University, Sendai 980-8578, Japan*

⁵*Advanced Light Source, Lawrence Berkeley National Laboratory, Berkeley, California 94720, USA*

(Received 23 June 2010; revised manuscript received 3 November 2010; published 16 March 2011)

We have performed a systematic photoemission study of the chemical-potential shift as a function of carrier doping in a pnictide system based on BaFe_2As_2 . The experimentally determined chemical-potential shift is consistent with the prediction of a rigid band shift picture by renormalized first-principle band calculations. This leads to an electron-hole asymmetry (EHA) in the Fermi surface (FS) nesting condition due to different effective masses for different FS sheets, which can be calculated from the Lindhard function of susceptibility. This built-in EHA, which matches well the observed asymmetric superconducting domes in the phase diagram, strongly supports FS quasineesting driven superconductivity in iron pnictides.

DOI: [10.1103/PhysRevB.83.094522](https://doi.org/10.1103/PhysRevB.83.094522)

PACS number(s): 74.70.Xa, 79.60.-i, 71.30.+h

I. INTRODUCTION

Even though the detail of the pairing mechanism in the recently discovered iron-based superconductors is still under intense debate, several theoretical investigations¹⁻⁵ and experimental observations,⁶⁻¹⁰ strongly suggest the importance of inelastic interband scattering between hole and electron Fermi surface (FS) pockets connected via the antiferromagnetic (AF) wave vector. Within this framework, the pairing strength depends on near- or quasineesting, here defined as a large enhancement of the spin susceptibility at a well-defined wave vector.⁵ The quasineesting conditions depend on the shape and size of the various FS pockets, which are tuned by the position of the chemical potential. The evolution of the chemical potential with carrier concentration is thus a key issue to understand the evolution of FS quasineesting and superconductivity in these materials.

The 122 structural phase of BaFe_2As_2 is particularly suitable for a systematic study of the chemical-potential shift since it can be doped either by electrons or holes following $\text{Fe}^{2+} \rightarrow \text{Co}^{3+}$ or $\text{Ba}^{2+} \rightarrow \text{K}^+$ partial substitutions, respectively. Interestingly, the electron- and hole-doped sides of the phase diagram show some noticeable differences. For example, while the maximum T_c value for the hole-doped side reaches 37 K at ambient pressure, it tops around 25 K for the electron-doped systems. Similarly, the superconducting dome extends to much higher doping in the hole-doped case, with an optimal concentration of around 0.2 hole/Fe against 0.08 electron/Fe for the electron-doped side.

Angle-resolved photoemission spectroscopy (ARPES) is a powerful tool to access directly the electronic structure with respect to the chemical potential. Our previous ARPES studies have already revealed strong variations in the pairing strengths associated with the various FS sheets in the electron-doped compounds⁹ as compared to the hole-doped ones,^{6,11} as well as the deterioration of the quasineesting conditions in highly overdoped samples for which T_c vanishes or is significantly suppressed.^{8,12} Although quasineesting was naturally proposed

to explain these anomalies, this concept has not been linked to the origin of the electron-hole asymmetry (EHA) and up to date there is still no systematic investigation of the impact of the chemical-potential shift on the band structure throughout the whole phase diagram.

Here we report a systematic ARPES study of the chemical potential as a function of carrier doping in the 122 pnictides. With doping, the chemical potential moves smoothly with respect to the low-energy valence states, in agreement with our local density approximation (LDA) calculations. However, we observed anomalously larger (smaller) core level shift than the valence band shift on the hole (electron)-doped side for the relatively undisturbed As $3d$ core levels, possibly due to the screening effect which increases (decreases) the core level shifts upon hole (electron) doping. Based on a rigid band shift approximation justified by our experimental results, we computed the doping dependence of the Lindhard spin susceptibility at the AF wave vector, and found that the Lindhard function itself is asymmetric as a function of doping, in a similar fashion as the asymmetry between the hole and electron superconducting domes. This strongly supports FS-quasineesting-enhanced superconductivity in the pnictides.

II. EXPERIMENT

The high-quality single crystals of the 122 series used in this study were grown by the flux method.¹³ Low-energy electron diffraction on mirrorlike cleaved surfaces shows a sharp 1×1 pattern in the nonmagnetic phase. High-resolution (4–20 meV) ARPES measurements of the low-energy electronic structure were performed in the photoemission laboratory of Tohoku University using a microwave-driven helium source ($h\nu = 21.218$ eV) and core level studies were done at the Synchrotron Radiation Center and the Advanced Light Source in the United States, as well as at the Photon Factory in Japan, using various photon energies. Our experiments have been performed using high-efficiency VG-Scienta SES-100, SES-2002, and R4000 electron analyzers. Samples were

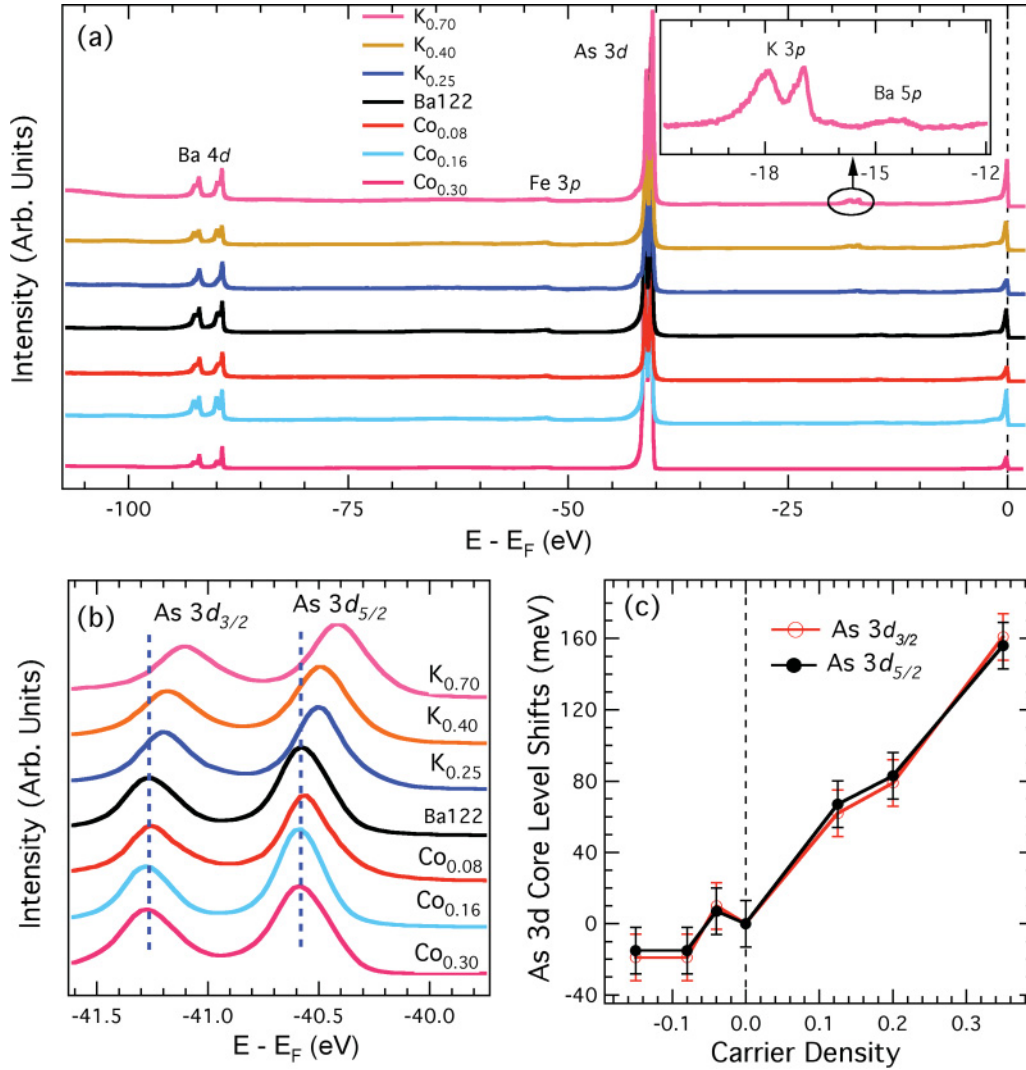


FIG. 1. (Color online) (a) Core levels of the Ba122 series recorded with a photon energy of 140 eV. The inset shows a zoom of the core levels of the $K_{0.70}$ sample in the 12–21 eV binding energy range. (b) Zoom of the As 3d core levels. (c) Doping dependence of the As $3d_{3/2}$ and As $3d_{5/2}$ core level energies as a function of carrier density (dopant per Fe). We evaluated the maximum position of the peaks by using Lorentzian fits around the peak maxima. Error bars are estimated by considering the uncertainty of the peak position and energy resolution of the measurement.

cleaved *in situ* and measured at 7–40 K in a vacuum better than 1×10^{-10} torr. The samples have been found to be very stable and without degradation for the typical measurement period of 20 h.

III. RESULTS AND DISCUSSION

Photoemission allows measurement of the core level states relative to the chemical potential. It has been used widely in the past to study the chemical-potential shift in high- T_c cuprates.^{14–16} Figure 1(a) shows a comparison of the core levels in the 0–110 eV binding energy range of seven samples distributed in the electron-doped and hole-doped sides of the phase diagram. These samples are $BaFe_{1.70}Co_{0.30}As_2$ ($T_c = 0$ K), $BaFe_{1.84}Co_{0.16}As_2$ ($T_c = 20$ K), $BaFe_{1.92}Co_{0.08}As_2$ ($T_c = 0$ K), $Ba_2Fe_2As_2$ ($T_c = 0$ K), $Ba_{0.75}K_{0.25}Fe_2As_2$ ($T_c = 26$ K), $Ba_{0.60}K_{0.40}Fe_2As_2$ ($T_c = 37$ K), and $Ba_{0.30}K_{0.70}Fe_2As_2$ ($T_c = 22$ K). For simplicity, hereafter we call them $Co_{0.30}$,

$Co_{0.16}$, $Co_{0.08}$, Ba122, $K_{0.25}$, $K_{0.40}$, and $K_{0.70}$, respectively. From low to high binding energies, we observed the Fe 3d (around the Fermi level), Ba 5p (~ 14.5 eV), K 3p (~ 18 eV), As 3d (~ 40.4 and 41.3 eV), and Ba 4d (~ 89.5 and 92 eV) states, respectively. In particular, the As 3d peaks are very strong in all compounds regardless of Co and K doping. Based on a previous photoemission study¹⁷ that indicates that the As atoms in $BaFe_2As_2$ are not perturbed significantly at the cleaved surface, we used the As 3d core levels to investigate the doping dependence of the chemical potential. In Fig. 1(b), we show a zoom of the As 3d core levels of all compounds. The position of the peaks moves toward the lower binding energies as K concentration increases. In contrast, the peak positions are almost unaffected by Co doping. We plot in Fig. 1(c) the shift of the As $3d_{3/2}$ and As $3d_{5/2}$ levels as a function of carrier density per Fe. We note that the variation of line shape in As 3d levels and weight of the Fe 3d peaks with doping which may be due to surface effects.

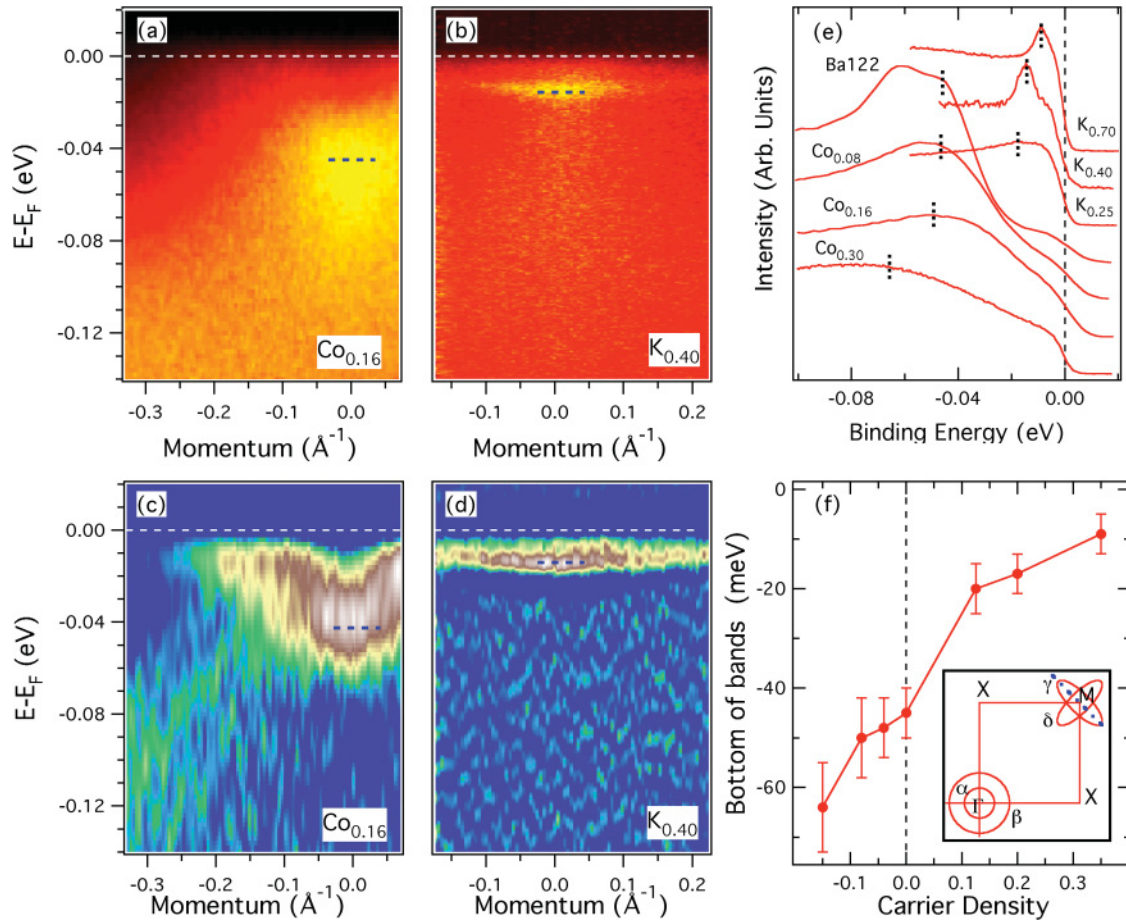


FIG. 2. (Color online) (a) and (b) ARPES intensity plots of the Co_{0.16} and K_{0.40} samples, respectively, along a cut passing through M, as indicated by a dashed line in the inset of panel (f). (c) and (d) Corresponding second derivative intensity plots. (e) EDCs for all seven samples showing the bottom of the γ electron band at the M point, as indicated by dashed lines. (f) Bottom of the electron bands versus carrier density.

An alternative and more direct determination of the chemical-potential shift is obtained by looking at the band dispersion near the Fermi level (E_F). In Figs. 2(a) and 2(b), we present ARPES intensity plots of the Co_{0.16} and K_{0.40} samples along a cut passing through M, as indicated in the inset of Fig. 2(f). The corresponding second derivative intensity plots are displayed in Figs. 2(c) and 2(d). The blue dashed lines are guides to the eye indicating the bottom of the upper electron band [the γ band as defined in Ref. 18, which can also be obtained by the energy distribution curves (EDCs) at the M point, which are given in Fig. 2(e)]. The bottom of this electron band at the M point moves down from E_F as the signed concentration decreases (more electrons), which is what we expect from simple band filling. In particular, this behavior supports the assumption that the Fe \rightarrow Co substitution electron-dopes the Fe layer, in contrast to a recent density functional theory calculation suggesting that Co and Ni only act as scattering centers in the Fe planes.¹⁹ Figure 2(f) summarizes our results on the seven differently doped samples.

Since the Ba-122 family is a multiband system, the rigid band scenario can be applied only if all bands evolve similarly upon doping. For this purpose, we compare in Fig. 3(a) fits of the α and β bands near the Γ point for three different

dopings: Co_{0.30}, Co_{0.15} (from our earlier paper⁸), and K_{0.25}. Even though the top of the α band is not observed in the latter case, the relative chemical-potential shift can be estimated by matching the slopes of the α and β bands. This method, which worked well in other systems,^{8,20} leads to a chemical-potential shift of the holelike bands that is consistent with the one of the electronlike bands, thus validating our approximation of a rigid band model.

At this point, it is instructive to compare LDA calculations to the core level shifts and the shift of the bottom of the electron band, which corresponds to the chemical-potential shift in a rigid band picture. It is clear from Fig. 3(b) that the core level shift is not the same as the shift of the valence band, and the differences between them are larger on the hole-doped side, which will be discussed below. Interestingly, the theoretically calculated chemical-potential shift is very much consistent with the observed valence band shift when theoretical values are divided by 4 as shown in Fig. 3(c), which is understood in terms of the band renormalization reported in previous ARPES studies,^{8,9,12,18} This indicates that the shift of the valence band corresponds to the chemical-potential shift, and consequently, the rigid band picture derived from the renormalized band structure is valid as a first-order approximation. It is also worth noting that the chemical-potential shift is asymmetric with

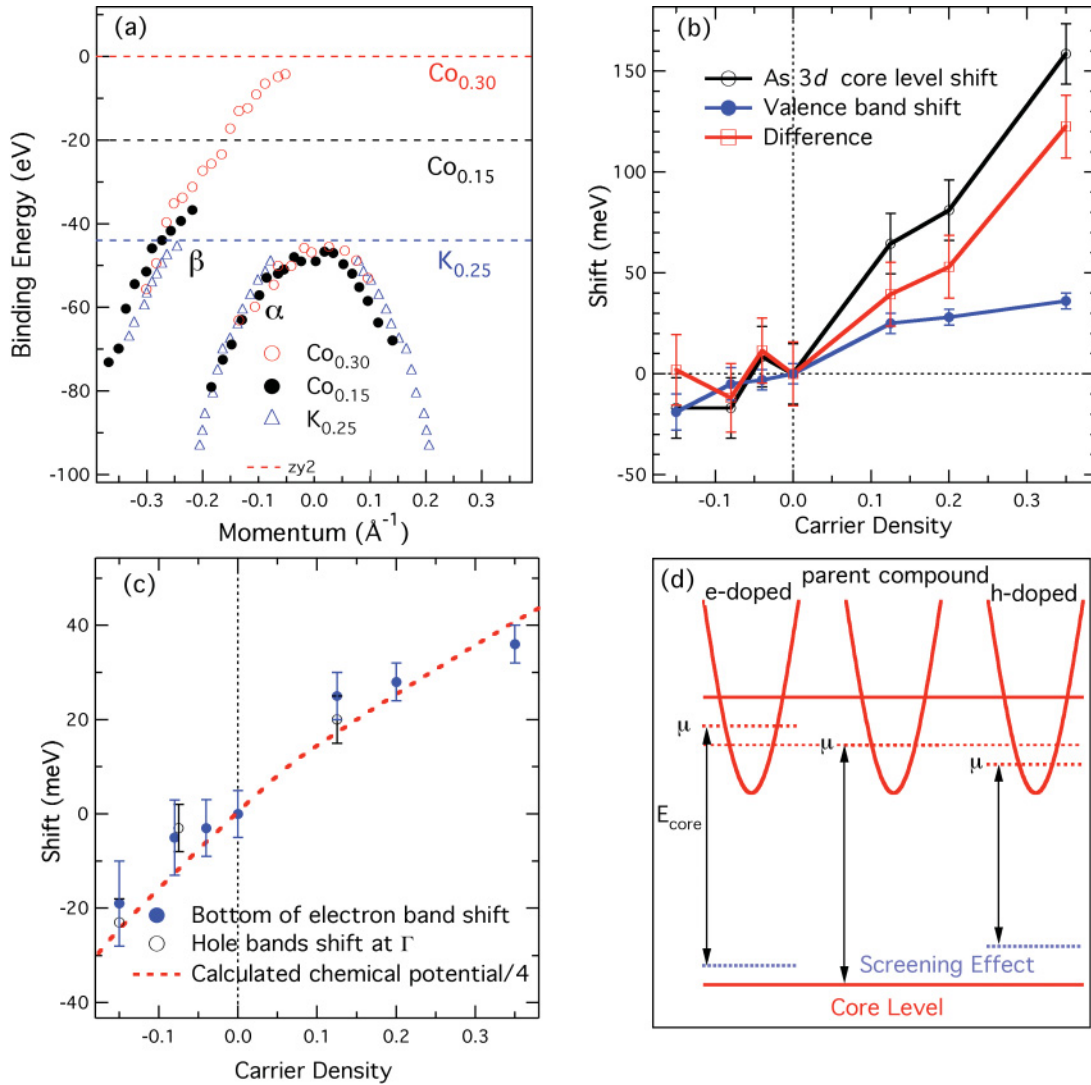


FIG. 3. (Color online) (a) Fits of the α and β bands for cuts passing through the Γ point. The bands have been shifted to match the band slopes. (b) Valence band and core level shifts as a function of the carrier density. The black curve with open circles shows the core level shifts while the blue curve with solid circles gives the valence band shifts measured from the band bottom. The red curve with open squares gives the difference between the core level and chemical-potential shifts. (c) The blue dots are the valence band shifts shown in panel (a) and the red dash curve is the LDA calculated values of the chemical potential divided by a factor of 4. The black dots correspond to the relative shifts derived from panel (a), with the shift of the Co_{0.30} compound fixed arbitrarily on the renormalized LDA curve. (d) Pictorial representation of the explanation of the core level and the chemical-potential shifts as a function of carrier density.

respect to zero doping. Both calculated and experimental data show that it is steeper on the electron-doped side of the phase diagram.

The core level shift can be understood as follows. The core level shift ΔE is related to the chemical-potential shift $\Delta\mu$ by the relation,

$$\Delta E = -\Delta\mu + K\Delta Q + \Delta V_M + \Delta E_R,$$

where ΔQ is the change in valency, K is a constant, ΔV_M is a shift due to change in the Madelung potential, and ΔE_R is the change in the core-carrier screening.²¹ Doping is not expected to change the As valency much. This implies that the term $K\Delta Q$ can be neglected. Therefore, the difference between the core level and the chemical-potential shift represented in Fig. 3(b) by the red curve is mainly related to ΔV_M and ΔE_R .

It is known that the screening term ΔE_R is proportional to the mobile carrier concentration, thus one expects that it has the same sign on the electron- and hole-doped sides and increases with doping. Such doping dependence of the screening term, as indicated in Fig. 3(d), will increase (reduce) the core level shift caused by the chemical-potential shift on the hole (electron)-doped side. This is consistent with our observation of different behaviors of the core level shift on the hole- and electron-doped sides. We note that the change of the Madelung term ΔV_M may not be the same on hole- and electron-doped sides, which can further enhance the difference of the core level shift on the two sides.

The above analysis suggests that a rigid band picture constitutes a good first approximation of the evolution of the chemical potential in the 122 family of iron pnictides. We now

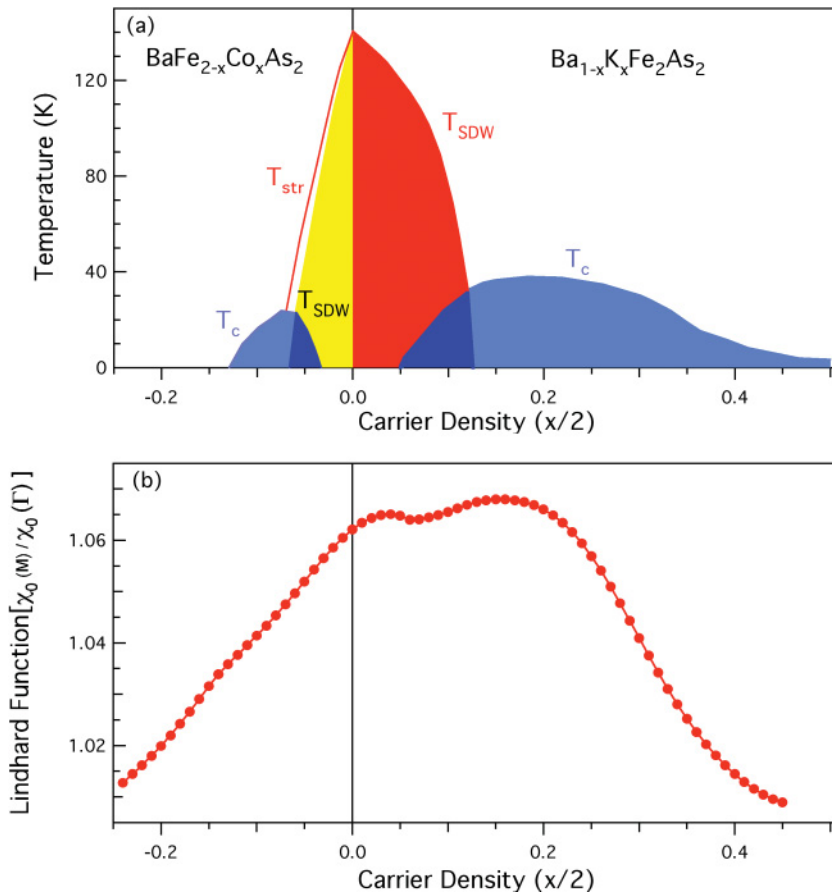


FIG. 4. (Color online) (a) Phase diagram of the hole- and electron-doped Ba-122 systems taken from Refs. 22 and 23, respectively. T_c , T_{SDW} , and T_{str} refer to the superconducting, the SDW, and the tetragonal to orthorhombic structural transitions, respectively. (b) Doping dependence of the Lindhard function at the M point (quasineesting wave vector) normalized by its value at the zone center. The Lindhard function was obtained by using LDA calculations.

ask a simple but fundamental question: is FS quasineesting able to explain the electron-hole asymmetry of the superconducting domes shown in the phase diagram of the 122 pnictides of Fig. 4(a)? To answer this question, it is necessary to compute the spin susceptibility. It is especially important to understand how the susceptibility evolves at the quasineesting (or AF) wave vector. We use the band structure calculated by LDA to compute the doping dependence of the Lindhard spin susceptibility at the quasineesting wave vector.^{24,25} We limit our calculations to the elastic component of the spin susceptibility. The results are displayed in Fig. 4(b). Interestingly, the hole- and electron-doped sides exhibit a strong asymmetry: while the Lindhard function decreases monotonically on the electron-doped side (with a small shoulder around ~ 0.12), it keeps a high value for a wide hole-doping range before starting to decrease. Remarkably, the maximum value of the calculated susceptibility is obtained near the experimental optimal hole doping, and the Lindhard function at the FS nesting wave vector tracks the superconducting transition qualitatively well. It is important to note that such an asymmetry in the Lindhard susceptibility would lead to a higher dielectric function and consequently to a larger screening effect on the hole-doped side. This is qualitatively consistent with the observed larger difference between the core level shift and the chemical-potential shift on the hole-doped side, as shown in Fig. 3(b). We caution that the nonmagnetic LDA calculations are no longer valid in the spin density wave (SDW) state because the band structure undergoes unconventional band folding that leads to the formation of Dirac cones.²⁶

The basic reason for electron-hole asymmetry in the calculated Lindhard function is as follows. The effective masses of the holelike bands, especially the β band, are larger than that of the electronlike bands at the M point, as observed by ARPES¹⁸ and quantum oscillation experiments.²⁷ To satisfy the Luttinger theorem, their top of band at zero doping must thus be closer to E_F than the bottom of the electron bands. Indeed, even for optimally hole-doped samples, the top of the α band is located only 25 meV above E_F .¹⁰ As a consequence, the holelike bands sink below E_F with electron doping much faster than the bottom of the electron bands are pushed above E_F with hole doping. Therefore, the FS quasineesting conditions are more robust in the hole-doped case. The built-in asymmetry of the FS quasineesting condition on the electron- and hole-doped sides offers a simple but powerful clue that the FS quasineesting with the AF wave vector triggers superconductivity in the pnictides.

IV. CONCLUSION

In conclusion, we have presented the doping dependence of the chemical potential in the 122 family of iron pnictides. As a first approximation, our results are consistent with a rigid band shift and with renormalized LDA calculations. The doping dependence of the As 3d core levels does not follow that of the chemical potential, suggesting a non-negligible screening effect. Within the rigid band shift approximation, the calculated Lindhard function at the FS-nesting wave vector reveals an electron-hole asymmetry

in the iron pnictides, which matches well with the observed electron-hole asymmetry of the superconducting domes in the phase diagram. Our findings reveal the importance of FS quasineesting in the pairing mechanism of the iron-based superconductors.

ACKNOWLEDGMENTS

This work was supported by grants from the National Science Foundation (NSF) and Department of Energy (DOE) of the United States; the Chinese Academy of Sciences, NSF,

and Ministry of Science and Technology of China; and the Japan Society for the Promotion of Science, Japan Science and Technology Agency (JST)–Transformative Research-project on Iron Pnictides (TRIP), JST–Core Research for Evolutional Science and Technology, and Ministry of Education, Culture, Sports, Science and Technology of Japan. This work is based upon research conducted at the Synchrotron Radiation Center supported by NSF Grant No. DMR-0537588, the Advanced Light Source supported by DOE Grant No. De-AC02-05CH11231, and the KEK-PF facility supported by Grant No. 2009S2-005.

-
- ¹I. I. Mazin, D. J. Singh, M. D. Johannes, and M. H. Du, *Phys. Rev. Lett.* **101**, 057003 (2008).
- ²K. Kuroki, S. Onari, R. Arita, H. Usui, Y. Tanaka, H. Kontani, and H. Aoki, *Phys. Rev. Lett.* **101**, 087004 (2008).
- ³F. Wang, H. Zhai, Y. Ran, A. Vishwanath, and D.-H. Lee, *Phys. Rev. Lett.* **102**, 047005 (2009).
- ⁴K. Seo, B. A. Bernevig, and J. Hu, *Phys. Rev. Lett.* **101**, 206404 (2008).
- ⁵V. Cvetkovic and Z. Tesanovic, *Europhys. Lett.* **85**, 37002 (2009).
- ⁶H. Ding, P. Richard, K. Nakayama, K. Sugawara, T. Arakane, Y. Sekiba, A. Takayama, S. Souma, T. Sato, T. Takahashi, Z. Wang, X. Dai, Z. Fang, G. F. Chen, J. L. Luo, and N. L. Wang, *Europhys. Lett.* **83**, 47001 (2008).
- ⁷A. D. Christianson, E. A. Goremychkin, R. Osborn, S. Rosenkranz, M. D. Lumsden, C. D. Malliakas, I. S. Todorov, H. Claus, D. Y. Chung, M. G. Kanatzidis, R. I. Bewley, and T. Guidi, *Nature (London)* **456**, 930 (2008).
- ⁸Y. Sekiba, T. Sato, K. Nakayama, K. Terashima, P. Richard, J. H. Bowen, H. Ding, Y.-M. Xu, L. J. Li, G. H. Cao, Z.-A. Xu, and T. Takahashi, *New J. Phys.* **11**, 025020 (2009).
- ⁹K. Terashima, Y. Sekiba, J. H. Bowen, K. Nakayama, T. Kawahara, T. Sato, P. Richard, Y.-M. Xu, L. J. Li, G. H. Cao, Z.-A. Xu, H. Ding, and T. Takahashi, *Proc. Natl. Acad. Sci. USA* **106**, 7330 (2009).
- ¹⁰P. Richard, T. Sato, K. Nakayama, S. Souma, T. Takahashi, Y.-M. Xu, G. F. Chen, J. L. Luo, N. L. Wang, and H. Ding, *Phys. Rev. Lett.* **102**, 047003 (2009).
- ¹¹K. Nakayama, T. Sato, P. Richard, Y.-M. Xu, Y. Sekiba, S. Souma, G. F. Chen, J. L. Luo, N. L. Wang, H. Ding, and T. Takahashi, *Europhys. Lett.* **85**, 67002 (2009).
- ¹²T. Sato, K. Nakayama, Y. Sekiba, P. Richard, Y.-M. Xu, S. Souma, T. Takahashi, G. F. Chen, J. L. Luo, N. L. Wang, and H. Ding, *Phys. Rev. Lett.* **103**, 047002 (2009).
- ¹³G. F. Chen, Z. Li, J. Dong, G. Li, W. Z. Hu, X. D. Zhang, X. H. Song, P. Zheng, N. L. Wang, and J. L. Luo, *Phys. Rev. B* **78**, 224512 (2008).
- ¹⁴K. Maiti, J. Fink, S. deJong, M. Gorgoi, C. Lin, M. Raichle, V. Hinkov, M. Lambacher, A. Erb, and M. S. Golden, *Phys. Rev. B* **80**, 165132 (2009).
- ¹⁵H. Yagi, T. Yoshida, A. Fujimori, Y. Kohsaka, M. Misawa, T. Sasagawa, H. Takagi, M. Azuma, and M. Takano, *Phys. Rev. B* **73**, 172503 (2006).
- ¹⁶N. Harima, A. Fujimori, T. Sugaya, and I. Terasaki, *Phys. Rev. B* **67**, 172501 (2003).
- ¹⁷S. deJong, Y. Huang, R. Huisman, F. Masee, S. Thirupathaiah, M. Gorgoi, F. Schaeffers, R. Follath, J. B. Goedkoop, and M. S. Golden, *Phys. Rev. B* **79**, 115125 (2009).
- ¹⁸H. Ding, K. Nakayama, P. Richard, S. Souma, T. Sato, T. Takahashi, M. Neupane, Y.-M. Xu, Z.-H. Pan, A. V. Federov, Z. Wang, X. Dai, Z. Fang, G. F. Chen, J. L. Luo, and N. L. Wang, e-print [arXiv:0812.0534](https://arxiv.org/abs/0812.0534) (to be published).
- ¹⁹H. Wadati, I. Elfimov, and G. A. Sawatzky, *Phys. Rev. Lett.* **105**, 157004 (2010).
- ²⁰K. M. Shen, F. Ronning, D. H. Lu, W. S. Lee, N. J. C. Ingle, W. Meevasana, F. Baumberger, A. Damascelli, N. P. Armitage, L. L. Miller, Y. Kohsaka, M. Azuma, M. Takano, H. Takagi, and Z.-X. Shen, *Phys. Rev. Lett.* **93**, 267002 (2004).
- ²¹S. Hüfner, *Photoelectron Spectroscopy* (Springer-Verlag, Berlin, 1995).
- ²²M. Rotter, M. Pangerl, M. Tegel, and D. Johrendt, *Angew. Chem. Int. Ed.* **47**, 7947 (2008).
- ²³D. K. Pratt, W. Tian, A. Kreyssig, J. L. Zarestky, S. Nandi, N. Ni, S. L. Bud'ko, P. C. Canfield, A. I. Goldman, and R. J. McQueeney, *Phys. Rev. Lett.* **103**, 087001 (2009).
- ²⁴G. Xu, H. Zhang, X. Dai, and Z. Fang, *Europhys. Lett.* **84**, 67015 (2008).
- ²⁵G. T. Wang, Y. Qian, G. Xu, X. Dai, and Z. Fang, *Phys. Rev. Lett.* **104**, 047002 (2010).
- ²⁶P. Richard, K. Nakayama, T. Sato, M. Neupane, Y.-M. Xu, J. H. Bowen, G. F. Chen, J. L. Luo, N. L. Wang, X. Dai, Z. Fang, H. Ding, and T. Takahashi, *Phys. Rev. Lett.* **104**, 137001 (2010).
- ²⁷J. G. Analytis, J.-H. Chu, R. D. McDonald, S. C. Riggs, and I. R. Fisher, *Phys. Rev. Lett.* **105**, 207004 (2010).